On the Effective Capacity of the Dense-Water Reservoir for the Nordic Seas Overflow: Some Effects of Topography and Wind Stress

JIAYAN YANG AND LAWRENCE J. PRATT

Department of Physical Oceanography, Woods Hole Oceanographic Institution, Woods Hole, Massachusetts

ABSTRACT

The overflow of the dense water mass across the Greenland–Scotland Ridge (GSR) from the Nordic Seas drives the Atlantic meridional overturning circulation (AMOC). The Nordic Seas is a large basin with an enormous reservoir capacity. The volume of the dense water above the GSR sill depth in the Nordic Seas, according to previous estimates, is sufficient to supply decades of overflow transport. This large capacity buffers overflow's responses to atmospheric variations and prevents an abrupt shutdown of the AMOC. In this study, the authors use a numerical and an analytical model to show that the effective reservoir capacity of the Nordic Seas is actually much smaller than what was estimated previously. Basin-scale oceanic circulation is nearly geostrophic and its streamlines are basically the same as the isobaths. The vast majority of the dense water is stored inside closed geostrophic contours in the deep basin and thus is not freely available to the overflow. The positive wind stress curl in the Nordic Seas forces a convergence of the dense water toward the deep basin and makes the interior water even more removed from the overflow-feeding boundary current. Eddies generated by the baroclinic instability help transport the interior water mass to the boundary current. But in absence of a robust renewal of deep water, the boundary current weakens rapidly and the eddy-generating mechanism becomes less effective. This study indicates that the Nordic Seas has a relatively small capacity as a dense water reservoir and thus the overflow transport is sensitive to climate changes.

1. Introduction

The North Atlantic Deep Water (NADW) is the main component of the vast water mass that fills the global deep ocean. A major portion of the NADW can be traced to the Nordic Seas and the Arctic Ocean where an intense surface cooling transforms the Atlantic-origin water to the prototype of the NADW. The cooled water, typically with a density greater than 1027.8 kg m^{-3}, spills over the Greenland–Scotland Ridge (GSR), mixes with the ambient North Atlantic Ocean Water at shelf breaks, and descends into the deep North Atlantic Ocean (Price and Baringer 1994). The overflowed water feeds the deep western boundary current (DWBC) and drives the lower limb of the Atlantic meridional overturning circulation (AMOC).

So the stability of the AMOC is intimately tied to a stable overflow transport. In this study we examine how the overflow stability is affected by wind stress and bathymetry.

The overflow transport from the Nordic Seas is about 6 Sv (1 Sv $\equiv 10^6$ m^3 s^{-1}) and is split roughly even on both sides of Iceland (Hansen et al. 2008). The Denmark Strait (DS) and Faroe Bank Channel (FBC) are the two deepest passages with sill depth of about 620 and 840 m, respectively. They are the two main conduits for the Nordic Seas overflow. Transport over the Iceland–Faroe Ridge (IFR), with a sill depth of about 480 m, makes a smaller contribution. Despite climate variations the overflow transport has remained stably strong without significant trends over the last a few decades (Hansen and Østerhus 2007; Olsen et al. 2008; Serra et al. 2010). With projections of accelerating changes in polar regions, one would wonder if the overflow could remain strong in the coming decades, and if not, how the AMOC would respond.

Corresponding author address: Jiayan Yang, Department of Physical Oceanography, Woods Hole Oceanographic Institution, Woods Hole, MA 02543.
E-mail: jyang@whoi.edu

The Nordic Seas overflow is hydraulically controlled and its transport depends on h_u—the height of the dense-water interface over the sill depth in the upstream basin (Whitehead et al. 1974; Pratt and Whitehead 2008; Girton et al. 2006; Nikolopoulos et al. 2003). The hydraulics prevents an unconstrained outflow to the Atlantic Ocean. The relationship between transport and h_u indicates that the present reservoir volume, that is, the amount of the dense water above the GSR sill depth, could supply multiple years and even decades of stable overflow transport without renewal of the source water (Käse 2006; Hansen and Østerhus, 2000; Hansen et al. 2008). The Nordic Seas reservoir therefore plays a stabilizing role in the overflow stability. The premise in such estimations, however, is that all dense water above the sill depth is freely available for overflow transport. This assumption overlooks some fundamental dynamical principles that govern the ocean circulation. Large-scale flows in the Nordic Seas are nearly geostrophic and along isobaths (Nøst and Isachsen 2003). The water mass that is initially trapped inside a closed isobath, like the vast amount of water that is stored in the interior deep basin, are not freely available to the nearly geostrophic boundary current that feeds the overflow. Some ageostrophic mechanisms or external forcing are needed to unlock the water mass that is trapped inside a closed geostrophic contour.

In this study, we will examine the effective capacity of the Nordic Seas reservoir by using a two-layer, nonlinear model. Our analyses and model results show that the amount of the dense water that is freely available to overflow is considerably smaller than the holding capacity. We will discuss how the wind stress forcing, eddy fluxes, and bathymetry affect the effective capacity of the Nordic Seas reservoir. The paper is organized as follows. A two-layer numerical model will be introduced in the next section. Model simulations using realistic and modified topographies will be presented and discussed in section 3 including some effects of wind, eddies, and bathymetry. A mass-budget model, modified from that used by Käse (2006), will be used in section 4 to discuss the time scales of the overflow drainage and the effective capacity of the reservoir. A summary and some further discussions will be included in section 5.

2. Model simulations

A two-layer and nonlinear numerical model, governed by the following equations, is used in simulating exchange between the lighter Atlantic water and the denser Nordic Seas water:

$$\frac{d\mathbf{u}_1}{dt} + f\mathbf{k} \times \mathbf{u}_1 = -g\nabla\eta - A\nabla^4\mathbf{u}_1$$
$$- [1 - H(h_2)]\frac{\lambda|\mathbf{u}_1|\mathbf{u}_1}{h_1} + \frac{\boldsymbol{\tau}_{\text{wind}}}{\rho h_1},$$

$$\frac{d\mathbf{u}_2}{dt} + f\mathbf{k} \times \mathbf{u}_2 = -g\nabla(\eta + \frac{\Delta\rho}{\rho}h_2) - A\nabla^4\mathbf{u}_2$$
$$- \frac{\lambda|\mathbf{u}_2|\mathbf{u}_2}{h_2} + [1 - H(h_1)]\frac{\boldsymbol{\tau}_{\text{wind}}}{\rho h_2},$$

$$\frac{\partial\eta}{\partial t} + \nabla \cdot (h_1\mathbf{u}_1 + h_2\mathbf{u}_2) = 0,$$

$$\frac{\partial h_2}{\partial t} + \nabla \cdot (h_2\mathbf{u}_2) = 0, \qquad (1)$$

where (u_n, v_n) and h_n are velocity and layer thickness in the nth layer ($n = 1, 2$ for the upper and lower layers, respectively), η is the sea surface height, $A = 5 \times 10^{10}$ m^4 s^{-1} is a biharmonic viscosity, $\lambda = -0.005$ is a quadratic bottom drag coefficient, and $\Delta\rho = 1/3$ kg m^{-3} is the water density difference between the two layers. The model allows outcropping of the lower layer ($h_1 = 0$) or grounding of the upper layer ($h_2 = 0$). The wind stress is applied to lower layer when it outcrops. Likewise, the bottom stress is used in the upper layer when it grounds. These situations are handled by the Heaviside Step Function $H(h_i)$ in Eq. (1) [$H(h_i) = 1$ if $h_i > 0$, and $H(h_i) = 0$ if $h_i \le 0$]. The model extends from 55° to 80°N with resolutions of $^1/_{12}°$ in the meridional direction and $^1/_6°$ in the zonal direction. The model uses both a realistic bathymetry, shown in Fig. 1a and idealized ones. In all experiments with realistic bathymetry, areas inshore of the 200-m isobath, which is indicated by the thick black line in Fig. 1a, are set to be land. (In other experiments we have moved the model boundary much closer to the actual shorelines and the evolutions of the overflow transport are basically the same.) The annual-mean wind stress, shown in Fig. 2a, is derived from a 23-yr (1988–present) daily climatology (Yu et al. 2008). The model uses a staggered C-grid and a time step of 6 s.

3. The capacity of the Nordic Seas as a dense-water reservoir

There are two different *capacities* of the dense-water reservoir. The first one is the *total capacity*—the volume of the dense water above the maximum GSR sill depth (840 m in the Faroe Bank Channel) inside the Nordic Seas. The second one is the *effective capacity*—the volume that is not prevented by conservative, nearly-geostrophic dynamics from overflowing the ridge. This capacity therefore depends on internal dynamical factors and external forcing. It is the effective capacity not
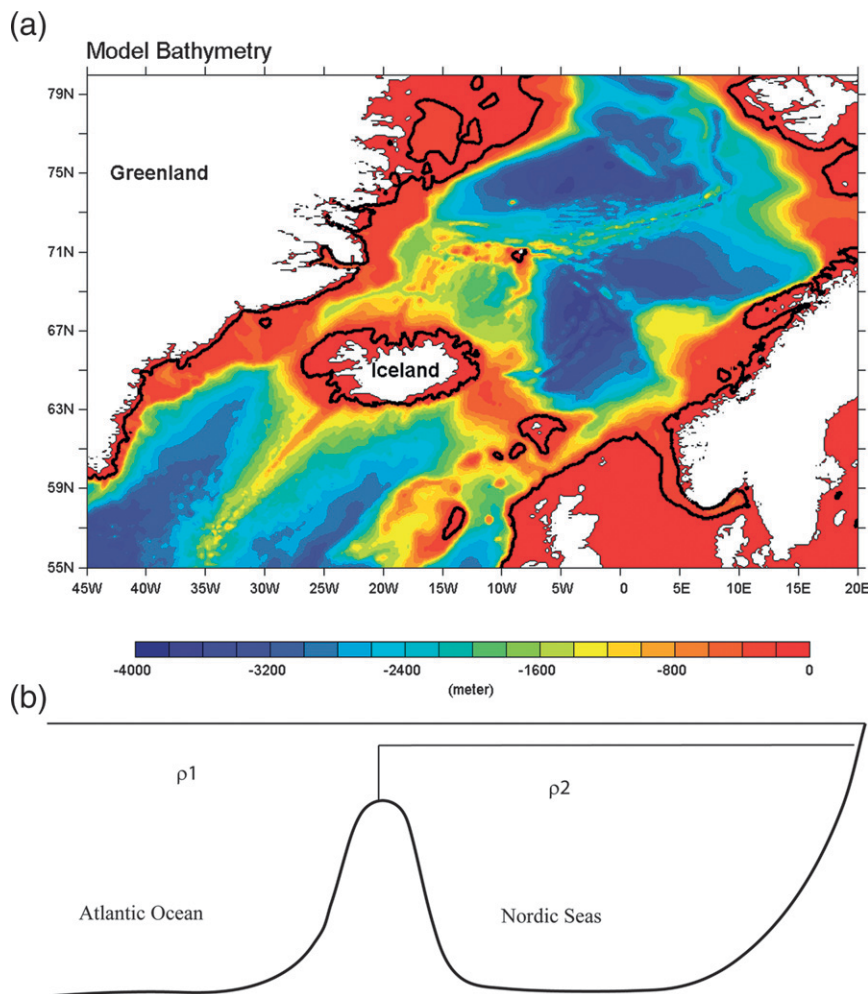
FIG. 1. (a) The model bathymetry. The thick black lines are 200-m isobaths that are used as the boundary in the model (shallower than 200 m is set to 0). (b) The initial model condition. The Nordic Seas is filled with dense water from bottom to 50 m below surface.

the total capacity that matters most to the immediate stability of overflows. In this study we will evaluate the effective capacity of the Nordic Seas by using "dam break" experiments similar to that conducted by Käse et al. (2009). To set up such experiments, the basin north of the GSR is filled with dense water (with density ρ_2) from the sea floor to 50 m below the surface (Fig. 1b and Fig. 2b). Elsewhere the model is filled initially with lighter water (ρ_1). No water-mass transformation, that is, diapycnal mass flux, is allowed during the simulations (so the total mass volume in each layer is conserved). The initial pressure difference across the ridge cannot be sustained as an equilibrium state. Topographic and Kelvin waves are generated once the initial dam is broken and the dense water is allowed to spill over the GSR into the Atlantic Ocean. This flow adjustment process is similar to the classical lock exchange experiment in a rotating system (Pratt and Whitehead 2008).

In our dam break experiments, the *initial* amount of the dense water above the sill (840 m) is 1.52×10^{15} m^3. This is large enough to supply nearly 10 years of a constant overflow transport of 5 Sv (in reality the transport will decrease as the height of dense-water layer h_u lowers). The result from the first dam break experiment is described in following. The annual-mean wind stress that is shown in Fig. 2a is applied in this experiment.

Snapshots of h_u (Figs. 2b–d) show that overflow draws dense water along geostrophic contours (isobaths) lowers h_u on the continental slope and results in a dome shape distribution with an elevated h_u in the interior deep basin. The overflow transports in DS (Q_{DS}), FBC (Q_{FBC}) and IFR (Q_{IFR}), vary significantly within the first month (black lines in Fig. 3), reaching the maximum transport of 2.32 Sv on the fourth day in DS, 5.44 Sv on the 13th day in FBC, and 1.22 Sv on the 25th day in IFR. The total overflow transport (Q_{total}) peaks at 6.6 Sv on
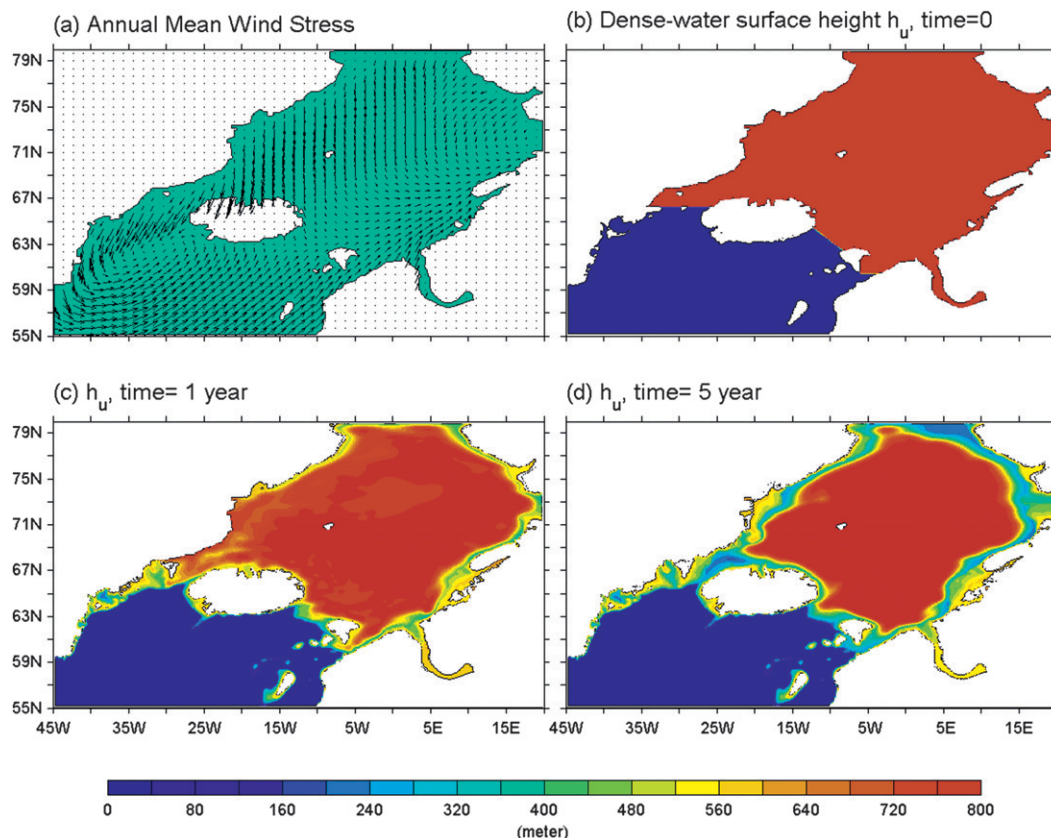
FIG. 2. (a) The surface wind stress used in the model; (b) the initial condition used in all experiments; (c) the height of the dense water in the first experiment after 1 year of simulation; and (d) at the end of fifth year. The overflow drains water around the periphery. The water mass in the interior is not affected by the overflow drainage.

the 13th day and then decreases rapidly afterward. At the end of first year, the transports have decreased to $Q_{DS} = 1.18$, $Q_{FBC} = 0.85$, $Q_{IFR} = 0.28$, and $Q_{total} = 2.31$ Sv. These represent reductions of 49%, 84%, 77% and 65% from their initial peak values. One year later at the end of second year, they were reduced by 90%, 93%, 84% and 88% from their initial peak values to $Q_{DS} = 0.23$, $Q_{FBC} = 0.36$, $Q_{IFR} = 0.20$, and $Q_{total} = 0.79$ Sv. The transports become virtually zero in all segments at the end of the fifth year. The pace of the reduction is in stark contrast to the expectation that the Nordic Seas is such an enormous reservoir that it can sustain a long period of robust overflow transport. The remaining deep water volume above the sill in the Nordic Seas, in contrast to transport reduction, remained large throughout the 10-yr simulation. It decreased merely 15% from its initial volume of 1.52×10^{15} m^3 to 1.29×10^{15} m^3 at the end of the fifth year when overflow is basically shut down. Five more years later at the end of the 10th year, it remained relatively high at 1.24×10^{15} m^3. So the reservoir's *effective capacity*, in this wind-driven two-layer overflow model, is only 15%–20% of the *initial capacity*

in the model. The reservoir appears to be a less stabilizing factor than what the total capacity would imply.

a. The role of wind stress forcing

What could have prevented 80%–85% of the dense water from immediately spilling over the ridge? The wind stress is the only external forcing in the model and so its effect will be scrutinized first. In our next experiment the wind stress forcing is turned off while everything else remains the same as in the first simulation. Without the wind stress forcing, Q_{DS} decreases more rapidly in the first 14 months (green line in Fig. 3a). This is consistent with previous findings (Serra et al. 2010) that cyclonic and barotropic wind-driven circulation contributes to the dense-water overflow through the Denmark Strait. After this initial period, however, Q_{DS} decreases at a slower pace than that in the wind-forced simulation (compared black and green lines in Fig. 3a). The overflow transport through the Faroe Bank Channel Q_{FBC} remains persistently higher than that from the wind-forced case (Fig. 3b). The transport of the dense water over the Iceland-Faroe Ridge Q_{IFR} is small in
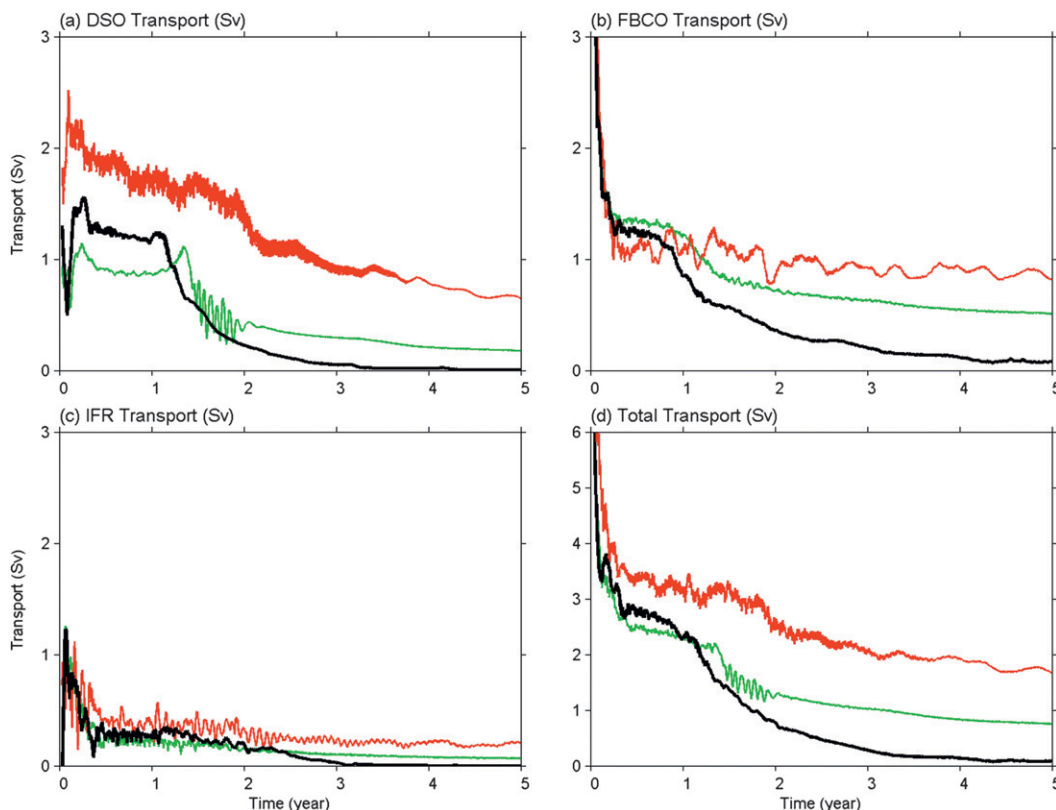
FIG. 3. Time series of overflow transports (black lines for the wind-driven experiment, green lines for the experiment without wind stress, and red lines for the experiment in which the maximum depth in the Nordic Seas is set to be 730 m). (a) Denmark Strait overflow; (b) the Faroe Bank Channel overflow; (c) transport over the Iceland-Faroe Ridge; and (d) the total transport.

either experiment (Fig. 3c). The total overflow transport Q_{total} decreases more slowly when the wind stress is removed (Fig. 3d). The height of the dense water surface over the sill depth at the end of the first and fifth years is shown in Fig. 4. Compared with the wind-forced case shown in Fig. 2, the amount of the dense water at the end of fifth year is clearly smaller in the present case without wind forcing. Does the wind stress forcing in the Nordic Seas act against the drainage of the dense water from the interior deep basin?

In the Nordic Seas the wind stress curl is positive and so the wind-driven circulation is cyclonic (Jonsson 1991). Our model uses both a realistic bathymetry and an observation-based wind stress. Both the bathymetry and the wind stress curl vary regionally on multiple spatial scales. The combination of those multiscale variations complicates the diagnosis of the leading dynamical processes. Our primary interest here is to understand how the overflow transport is affected by a wind stress with a positive curl in a more general two-layer exchange flow. A better understanding will therefore help diagnose the more complicated results discussed above.

With this in mind, we decide to conduct a set of idealized experiments.

In the following idealized experiments, we use the same two-layer, nonlinear model but formulate it in a Cartesian coordinate with a resolution of 5 km on a β plane centered at 65°N. Experiments were conducted in pairs, one with and the other without wind stress forcing. The bathymetry in the first set of idealized experiments is shown in Fig. 5a. Two circular basins are connected by a strait. The maximum depth is 1000 m and the minimum is 500 m over the whole model domain. The sill depth in the connecting strait is 500 m. The depth in the two circular basins increases linearly from 500 m at the boundary to 1000 m with a slope of 0.004. So the width of the slope region is 125 km. The depth and the size of the idealized basin are much smaller than that of the Nordic Seas and so the model results are relevant only qualitatively. Initially, eastern basin is filled by a denser water mass with a density of $\rho_2 = 1027.8$ kg m^{-3} to the level of 100 m below surface (or 400 m above the sill depth). The entire western basin and the connecting strait from the surface to the bottom and the upper 100 m
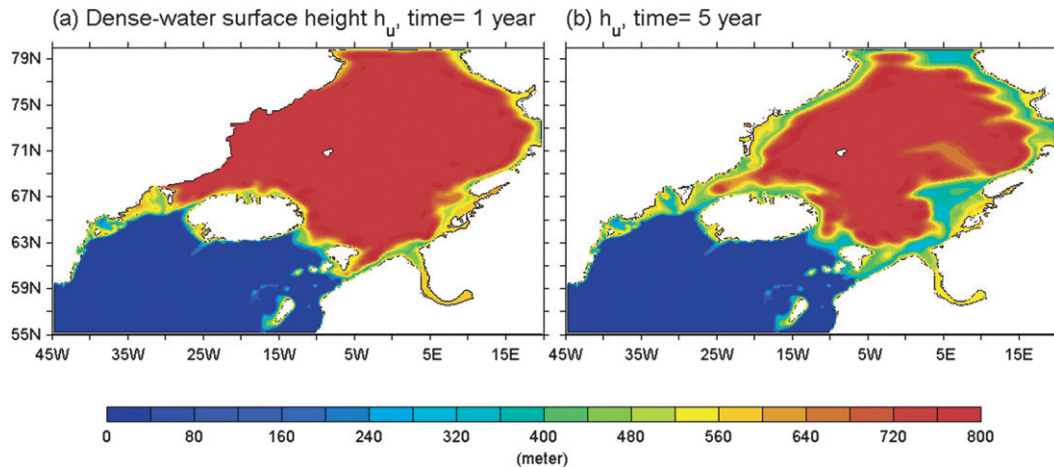
FIG. 4. As in Figs. 2c,d, except that the wind stress is removed. The water mass in the deep basin is more effectively drained.

in the eastern basin are filled with a lighter water mass with a density of $\rho_1 = \rho_2 - \Delta\rho$ (where $\Delta\rho = 1/3$ kg m^{-3}). The wind stress has only the zonal component and varies linearly from 0.5 dyn cm^{-2} at $y = 0$ to -0.5 dyn cm^{-2} at boundary $= 1000$ km (the red line in Fig. 5b). So the curl of the wind stress is positive and constant. We follow the same procedure as in the previous dam break experiments with realistic bathymetry (Figs. 1–4). The model is integrated forward from the initial condition described above. Two parallel experiments were conducted, one without wind stress and the other with wind stress applied in the eastern circular basin (the upstream basin for outflow of dense water). Wind stress is not applied in the western basin and in the strait in either experiment.

Because of the initial pressure difference between two basins, the dense water is flushed from the eastern to the western basin through the connecting strait. The transport, however, decreases rapidly within the first two months in both experiments. In the case without wind forcing, for example, the outflow transport reaches as high as 2.0 Sv at the end of the first day, decreases gradually to 1.4 Sv at the end of 30th day, and then rapidly to 0.2 Sv at the end of 50 days. The transport oscillates between 0.2 and 0.6 Sv with periods of about 35–45 days in the first year and then reaches a quasi-steady level of 0.15–0.2 Sv between year 2 and year 10 (the black line in Fig. 5f). The time scales of the initial adjustment and oscillations are set by Kelvin and topographic waves. They will be discussed further in section 3d.

Figure 5c shows the height of dense water surface over the sill depth at the end of the 10th year. This snapshot is taken long after the outflow transport has stabilized at about 0.15-Sv level. The dense-water mass in the deep

basin is largely untapped since h_u remains very close to 400 m above the sill depth—the level used in the initial condition. This is consistent with the experiments that used realistic bathymetry. In a parallel run, the wind stress that is shown by red line in Fig. 5b is applied in the eastern circular basin. The western basin and the connecting strait are not forced by wind stress. The outflow transport of the dense water from the eastern to the western basin (the red line in Fig. 5f) varies in the first year and rapidly diminishes to zero at the end of the third year. The thickness of the dense water layer is zero in the slope region in the upstream (eastern) basin.

It is interesting to note that h_u, that is, the height of the dense water surface, has been elevated above its initial height ($h_u = 400$ m) in the deep basin (Fig. 5d) in this experiment with a positive wind stress curl. This is different from the case without wind stress forcing (Fig. 5c) in which h_u at the end of the 10th year is close to the initial condition in the deep basin. So the wind stress must have forced a convergence of the dense water mass toward the deep basin. How can this be accomplished? Fig. 6a schematized this wind stress forcing mechanism. A positive wind stress curl forces a divergence in the surface Ekman transport and an upwelling of the deep water. The divergence results in surface water being pushed to side boundary. To compensate the mass flux and to feed the upwelling, there must be a convergence of the dense water mass in the lower layer toward the basin's interior. This would create a dome shape distribution of h_u. The convergence of the dense water toward the basin's interior also acts against the outward transport of the dense water to the overflow-feeding boundary current. So a wind stress with a positive curl makes the dense-water less available for the overflow and thus results in a smaller effective capacity of the reservoir.
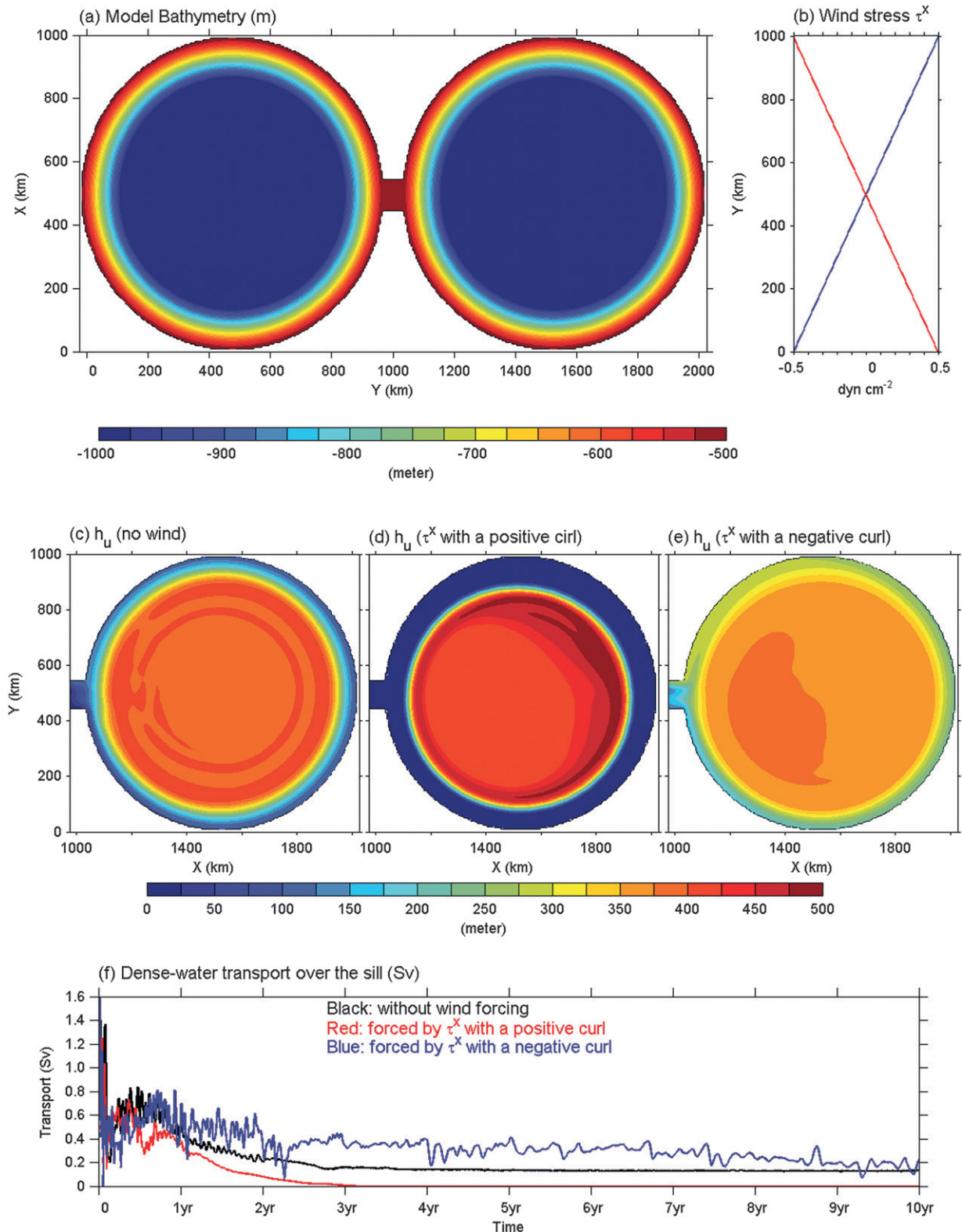
FIG. 5. A set of idealized experiments was conducted to investigate how wind stress curl affects the overflow in a dam break scenario. (a) The bathymetry (the slope is 0.004); (b) two wind stress profiles, one with a positive (red) and the other with a negative (blue) curl; (c) the height of the dense water surface over the sill h_u at the end of 10th year simulation from experiment that has no wind stress forcing; (d) h_u at the end of 10th year in the simulation with a positive wind stress; (e) h_u forced by a negative wind stress curl; and (f) the overflow transports from three experiments are shown.
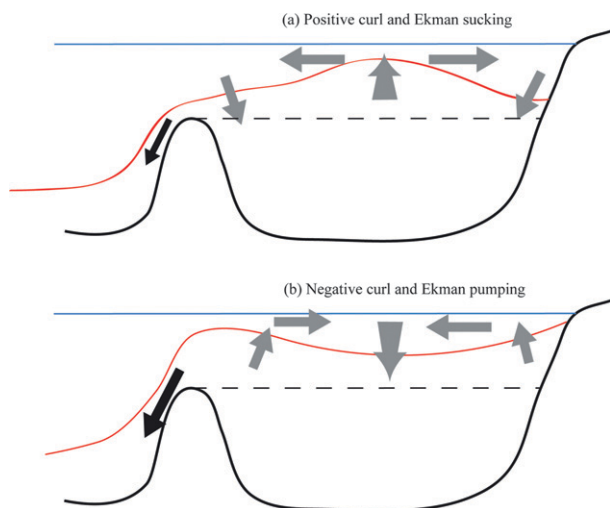
FIG. 6. Schematics of how wind stress curl affects the overflow transport: (a) for a positive curl and Ekman suction; and (b) for a negative curl and Ekman pumping basin is more effectively drained.

To further demonstrate the role of wind stress, we ran another experiment in which the model was forced by the opposite wind stress (blue line in Fig. 5b) that has a negative curl. The height of the dense water surface taken at the end of the 10th year indicates that the water in the interior basin is drained more effectively (Fig. 5e). The negative curl of the wind stress promotes the divergence of the dense water to the periphery where the water mass is transported by the boundary current to the overflow. This mechanism is schematized in Fig. 6b. The differences of the overflow transport and the effect of wind stress are further illustrated in the transport time series shown in Fig. 5f.

Figures 7a and 7b show the evolution of the layer interface along 75°N in the three experiments discussed above. The black lines represent the initial condition (i.e., h_u is 50 m below the sea surface in the Nordic Seas), and the red, blue, cyan, and magenta lines are the profiles of h_u at the end of first, second, fifth, and tenth year, respectively. In the two experiments with an unmodified bathymetry (Figs. 7a,b) the dense water is gradually drawn along the continental slope on the eastern side of the boundary as the layer interface flattens progressively with time. The interface slope along the western boundary is less changed (Figs. 7a,b). This is partly due to the western boundary current forced by the wind stress. As the outflow drains water along the slope, a dome-shape distribution of the pycnocline (the layer interface in the model) is formed as shown in Fig. 7. The shape of the pycnocline tends to propagate westward owing to the planetary β effect.

The role of the divergence in the Ekman transport, as schematized in Fig. 6a, is illustrated clearly Fig. 7a. The
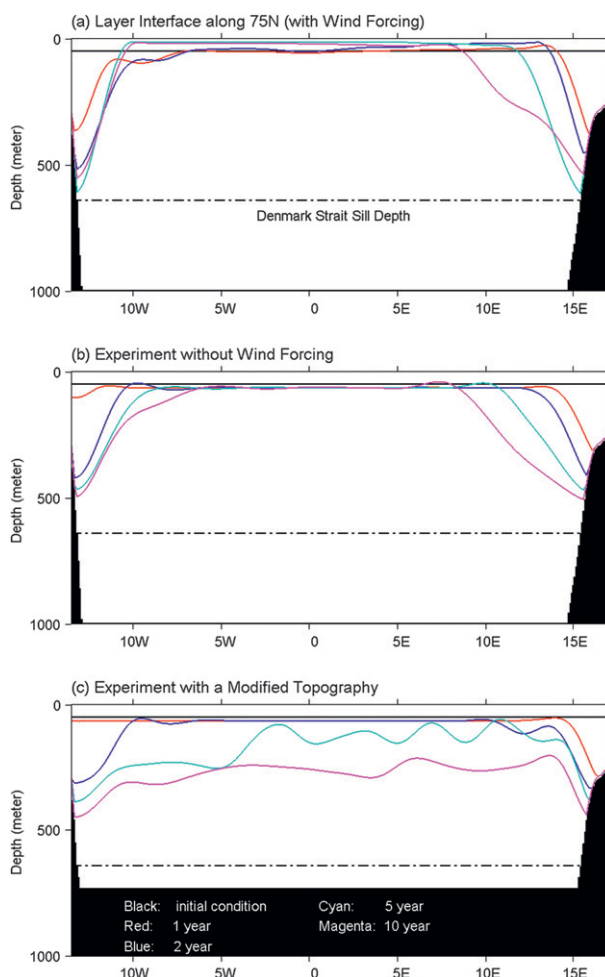

FIG. 7. The evolution of the dense-water surface along 75°N in three experiments that use realistic or modified Nordic Seas bathymetries.

height of the layer interface h_u was initially set at 50 m below sea surface (black line). But it increases after the dam is broken and the wind stress is applied. In fact, the lower layer nearly outcrops in the deep basin at the end of the fifth year. In contrast, h_u in the deep basin remains roughly at the same height as in the initial condition in the case without wind stress forcing (Fig. 7b).

b. Topographic effects

As shown above, a positive wind stress curl pushes the dense water toward the interior and makes it harder for the overflow-feeding boundary current to draw water from the deep basin. But the overflow transports still decrease rapidly even without wind forcing in both experiments with realistic and idealized bathymetry. In the experiment with a realistic bathymetry and wind stress, for instance, the total transport drops from the initial high of 6.5 Sv to about 0.75 Sv at the end of the fifth year

and to 0.5 Sv at the end of the 10th year (Fig. 3). So it is clear that the wind stress is not the only factor that restricts the overflow from the reservoir.

What else could prevent the overflow from draining the dense water stored in the deep basin? The overflow drains water mass mostly along isobaths on the continental slope. The water mass that is trapped inside a closed isobath is not freely available for nearly geostrophic flow. Ageostrophic processes, such as friction (through the bottom Ekman layer) and eddies, help break such containment. Would the effective capacity of the dense-water reservoir increase if we loosen the bathymetric constraint? In the next experiment the maximum depth in the Nordic Seas is set at 730 m as shown in Fig. 8a (regions where the depth is shallower than 730 m are not affected). We chose 730 m because it is the middle-depth level between 620 and 840 m, the sill depths in DS and FBC, respectively. The initial condition is the same as in the previous experiments, that is, h_u is 50 m below sea surface. No wind stress is used. The initial deep-water volume above the sill is $1.33 \times 10^{15} \, \text{m}^3$.

In comparison with the two previous experiments that use unmodified and realistic bathymetry (shown in Figs. 2 and 4), the overflow transport through the Denmark Strait Q_{DS} in this modified bathymetry experiment decreases considerably more slowly and remains relatively strong at 1.76 Sv after 1 year and at 0.65 Sv after 5 years (red line in Fig. 3a). Through most of the 10-yr simulation period, Q_{DS} is more than twice as large as that from the experiment without bathymetry modification (red and green lines). The situation in FBC, however, is different. In the first year Q_{FBC} was actually smaller than that with unchanged bathymetry (comparing red and green lines in Fig. 3b). But it remains quite steady at about 1 Sv afterward. The dense-water transport over the Iceland-Faroe Ridge is smaller in all cases and does not contribute much to the overall transport. The total transport has a maximum transport about 6.5 Sv (achieved on 15th day) similar to that in the previous experiment. It is reduced to 3.2 and 1.68 at the end of first and fifth year. This reduction rate is still rapid but considerably slower than that in the previous two cases.

Figures 8b and 8c show the surface height of the dense water (h_u) at the end of the first and fifth years. The water mass in the interior is clearly more drained in this experiment with a modified topography. The initial response at the end of the first year (Fig. 7b) is actually similar to the previous case shown in Fig. 4. Overflow drains water along the periphery. But as the model runs over a longer period of time, some major differences emerge. The dense-water mass in the interior is no longer restricted by bathymetry and moves more freely to the boundary current that feed into the overflow transport. The dense-water height h_u at the end of fifth year is lower over the whole Nordic Seas, not just along the slope as in the previous case. The volume of the dense water above the sill decreased from $1.33 \times 10^{15} \, \text{m}^3$ initially to $1.20 \times 10^{15} \, \text{m}^3$, $0.91 \times 10^{15} \, \text{m}^3$, and $0.72 \times 10^{15} \, \text{m}^3$ at end of first, fifth, and tenth year, respectively. These represent reductions of 9.8%, 31.6%, and 46% from the initial value. The effective capacity, if measured by the fraction of the water reservoir that has actually outflowed the Nordic Seas at the end of the 10th year, is almost a factor of three greater than that in the case with the wind stress forcing and a deep Nordic Seas (Fig. 2 and black lines in Fig. 3). Figure 7c shows the evolution of h_u along 75°N. The water mass in the interior deep basin is drawn as in the boundary region. So the height of the dense-water surface in the interior lowers progressively in time.

c. A role of eddies

Our numerical experiments showed that the dense water mass that is trapped inside a closed geostrophic contour in the Nordic Seas is not freely available for overflow. Ageostrophic processes or external forcing would be needed to move the dense water mass from the deep basin to the overflow-feeding boundary currents. Yang and Price (2000, 2007) analyzed the basin integral of the potential vorticity budget in a semienclosed marginal sea and used a one-layer numerical model to demonstrate that the overflow becomes more effective in draining the deep-basin water mass when the eddy viscosity is increased in a reduced-gravity model. Their model did not resolve eddies and the role of eddy fluxes was examined crudely by varying the model eddy viscosity. Spall (2004) used a high-resolution ocean general circulation model and demonstrated that the transport from the interior to the boundary current is carried out mainly by eddies that are generated by a baroclinically unstable boundary current.

The internal deformation radius is about 10 km along the continental slope. Our model permits and in fact does simulate eddies as shown in Fig. 4b. Why are eddies in our model insufficient to maintain a robust overflow transport? To address this issue we decide to conduct additional experiments by using idealized bathymetry. Some important topographic features, such as the slope steepness, can be varied more easily when using idealized bathymetries. In the next set of model experiments, the bathymetry is similar to that shown in Fig. 5 except that the steepness of the slope is changed.

Spall (2010) identified an important parameter, the width of the continental slope, for the stability of the boundary current. The continental slope in the Norwegian
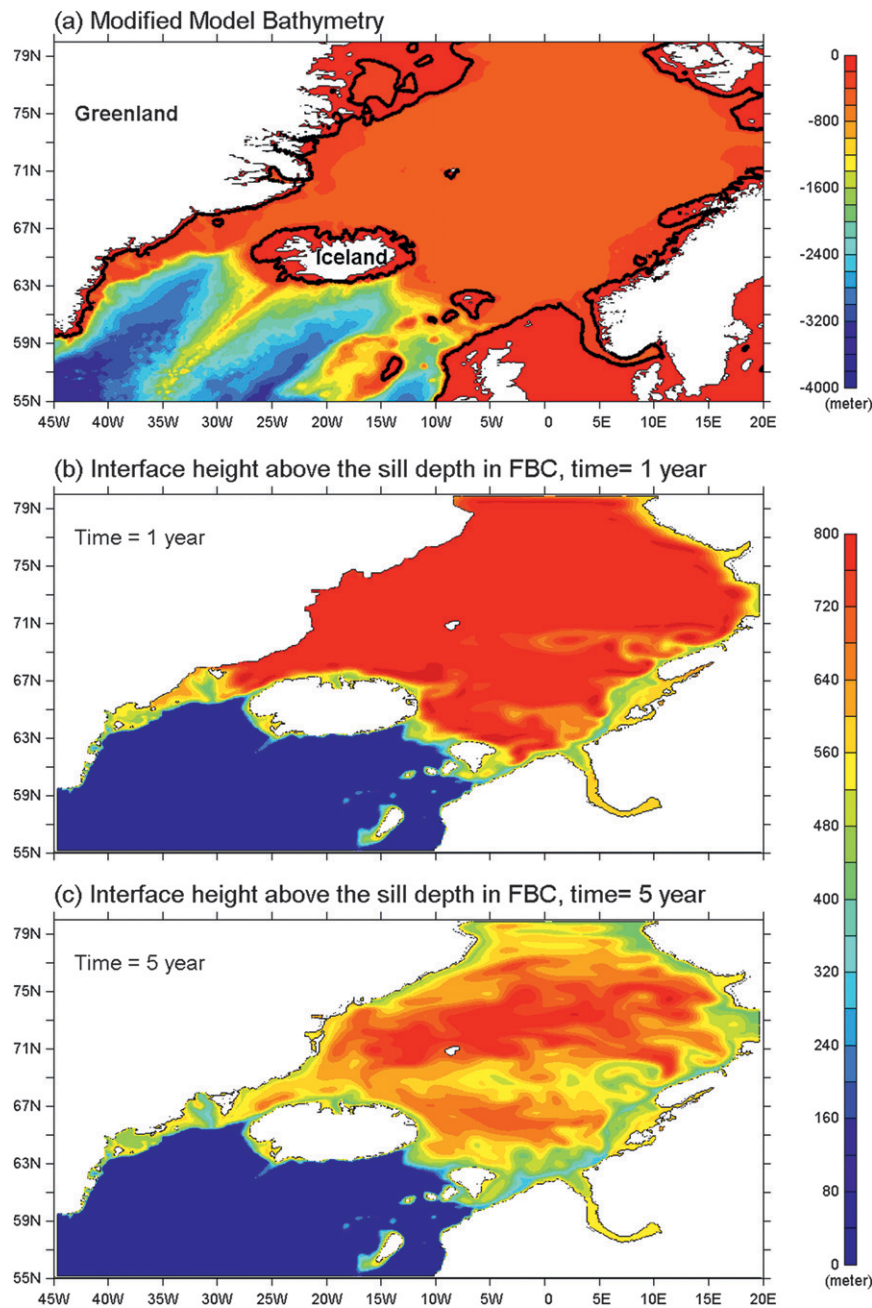
FIG. 8. (a) The modified bathymetry used in the third experiment. The dense-water height (b) at the end of the first year and (c) at the fifth year. When the topographic constraint is loosened, the interior water mass is effectively drained.

Sea, for example, is steep and narrow. The boundary current, which is strongly influenced by the spatial scale across the slope, becomes narrower and faster there. The increase of the velocity and its vertical shear makes the flow less stable baroclinically. Eddies generated by the baroclinic instability in such regions play a leading role in transporting dense water mass from interior to

the overflow-supplying boundary current. To test the Spall's mechanism, we increase the slope from 0.004 to 0.01. The width of the slope narrows from 125 to 50 km as shown in Fig. 9a. Two experiments were conducted, one with and the other without wind stress forcing. The zonal component that has a positive curl (the red line in Fig. 5b) is applied in the eastern basin in the wind-forced
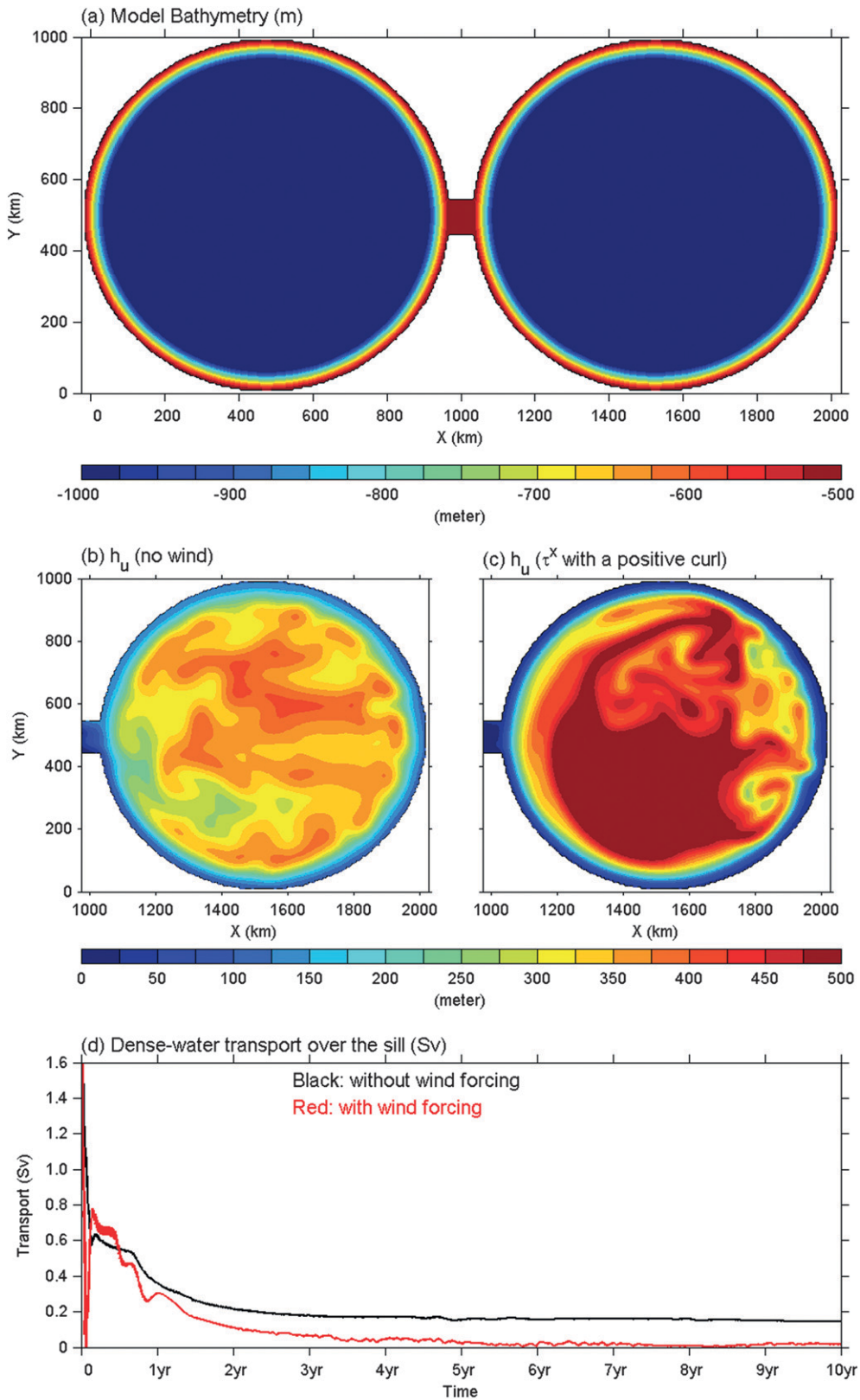
FIG. 9. A set of idealized experiments that use a steeper topographic slope than what is shown in Fig. 5. Eddies are present. But they do not fundamentally change the effective capacity of the reservoir.

run. Figures 9b and 9c show the height of the dense water surface over the sill depth at the end of the 10-yr runs. Eddies are clearly shown in both runs. Compared with the previous case with a less steep slope (Fig. 5), a greater amount of the dense water mass in the interior is drawn. The overflow transport drops rapidly from an initial high of about 2 Sv to about 0.6 Sv within the first month (black line in Fig. 9c) in the case without wind forcing, rebounds to 0.7 Sv and then decreases slowly to 0.2 Sv within three years. It remains at the low transport level of about 0.2 Sv in the remaining of the 10-yr simulation. Compared with the previous idealized experiment with a gentler slope (Fig. 5c), eddies are clearly present even at the end of 10th year simulation when the boundary current has substantially weakened. The volume of the dense water above the sill depth remains at 2.3×10^{14} m^3—almost 75% of the initial volume of 3.1×10^{14} m^3. In the case with wind stress forcing, the dense-water volume at the end of the 10th year (Fig. 9c) is even larger at 2.8×10^{14} m^3, which is 90% of the initial volume.

We have conducted experiments with even steeper slopes, the results remain qualitatively similar to that shown in Fig. 9. How do we reconcile the difference between our results and Spall's mechanism? A key difference is that the convection and thus the deep-water formation are always active in Spall's simulations. So the dense-water layer is continuously replenished. In our dam break experiments, no water-mass transformation is allowed. Initially, there is a steep isopycnal tilt when the boundary current draws the water mass along the slope. Eddies are active in fluxing the water mass to the boundary current. But the isopycnal tilt flattens gradually as the water mass in the vicinity of the slope is drawn. The sheer of the boundary current weakens and the boundary current becomes more stable baroclinically. In Spall's model, the continuous deep-water formation is able to maintain a steep isopycnal slope and keep the eddy generating mechanism effective throughout his simulations. Without the renewal of the dense water in the interior, the eddy flux plays only a limited role.

d. The initial adjustment process

In all experiments with either idealized or realistic bathymetries, the overflow transport is reduced sharply in the first one or two months. Taking the experiment shown in Fig. 5c with an idealized bathymetry and without wind stress forcing as an example, the rapid reduction in the transport begins between 30th and 50th day. Our analyses indicate that this time scale is set by an internal Kelvin wave. A linear baroclinic Kelvin wave in the model has a speed of about 0.91 m s^{-1} (for $\Delta\rho =$

1/3 kg m^{-3}) and would take about 40 days of propagation to complete one circumference of a circular basin. A baroclinic topographic Rossby wave, however, would take nearly two years to complete one circumference. The speed of a barotropic topographic Rossby wave, on the other hand, travels at a speed close to 30 m s^{-1} and would take less than 2 days to propagate once around a circular basin. It may contribute to the initial adjustment but is too fast to be associated with the 35–45 days oscillation.

Our diagnoses indicate that the height of the layer interface h_u decreases on the southern side of the strait entrance when the dam is broken and the dense water is flushed to the western basin. As the drainage continues, the h_u anomaly propagates cyclonically along the boundary in the upstream basin at an internal Kelvin wave speed. The outflow transport decreases gradually before the initial Kelvin completes its propagation around the boundary. When this initially generated Kelvin wave completes one cycle and reaches the northern side of the connecting strait, the pressure gradient, or the difference of h_u across the strait, drops and the geostrophic transport of the outflow starts a rapid reduction.

4. A water-mass budget/hydraulic model

The transport plots of Fig. 3 exhibit several time scales, including an initial steep drop on the scale of a month, followed in many cases by a secondary drop of 2–3 years. Käse (2006) formulated a simple mass budget model to predict a response time of one to multiple decades for deep waters of the Nordic Seas. We now examine his conclusions within the context of our own finding (of a shorter time scale) using an altered version of his model. Since we are concerned primarily with initial-value experiments, we remove his source term and replace his hydraulic transport relation, valid for a sill with a rectangular cross section, with the relation for a parabolic cross section (see Borenäs and Lundberg 1986, 1988). The latter is more easily fit to actual topography and avoids the complications posed by separation of the interface from a vertical sidewall. We also allow deep fluid to drain out through 2 straits. For the conditions assumed in the Käse (2006) model, the elevation of the interface (relative to the sill) in the interior of the basin is uniform. Absent any sources of deep fluid, the lower layer will drain according to the following statement of continuity:

$$A \frac{dh_{\text{FBC}}}{dt} = -\gamma_{\text{DS}}(h_{\text{FBC}} - \Delta)^2 - \gamma_{\text{FBC}} h_{\text{FBC}}^2. \quad (2)$$

Here A is the horizontal area occupied by the deep water, roughly 1.1×10^6 km^2. The two terms on the right-hand side give the volume outflow rates due to the Demark Strait and Faroe Bank Channels. In the parabolic sill formulation, these are proportional to the square of the elevation of the interior interface over the sill. Thus h_{FBC} is the elevation relative to the lowest point in the Faroe Bank Channel sill, and $h_{FBC} - \Delta$ is the elevation relative to the Denmark Strait sill, which is shallower than the former by amount $\Delta \cong 230$ m. The remaining coefficients are given by

$$\gamma_{FBC} = \left(\sqrt{\frac{3g'}{2\alpha}} \frac{1}{2+r} \right)_{FBC} \quad \text{and} \quad \gamma_{DS} = \left(\sqrt{\frac{3g'}{2\alpha}} \frac{1}{2+r} \right)_{DS},$$

where g' is the reduced gravity, α is the bottom curvature, and $r = f^2/g'\alpha$. Estimates for the curvature are $\alpha = 5.8 \times 10^{-6}$ m^{-1} for the Faroe Bank Channel sill and $\alpha = 1.3 \times 10^{-6}$ m^{-1} for the broader Denmark Strait sill [Borenäs and Lundberg (1988) and Killworth (1992)].

Equation (2) is considerably simplified if it is assumed that the two sill depths are the same ($\Delta = 0$), so that the two straits contribute equally to the drainage. A straightforward integration with initial condition $h_{FBC} = h_o$ leads to

$$\frac{h_o - h_{FBC}}{h_o h_{FBC}} = \frac{(\gamma_{FBC} + \gamma_{DS})t}{A}. \tag{3}$$

The time required to drain 95% is calculated by setting $h_{FBC} = 0.05 h_o$:

$$T_{95\%} = \frac{19A}{(\gamma_{FBC} + \gamma_{DS})h_o}, \tag{4}$$

with $g' = 4 \times 10^{-3}$ m s^{-2}, $f = 1.3 \times 10^{-4}$ s^{-1}, and $h_{uo} = 850$ m, we compute $T_{95\%} = 45$ yr, consistent with the order of magnitude found by Käse (2006). However, if we reduce the area A to that occupied within a Rossby deformation radius R_d of the coast, roughly $A_R = CR_d$, where $C \approx 2(\pi A)^{1/2}$ and we take $R_d = (g'h_{uo})^{1/2}/f$, then the drainage time is reduced to 2 years, which is more in line with our model results.

The total volume above sill level will eventually drain over a much longer time scale due to cross-isobath motion caused by friction or other ageostrophic effects, and there is an implied long-term buffering effect for water that is introduced into the interior of the basin, perhaps by deep convection. However, recent modeling studies (Spall 2004, 2010) have suggested that sinking occurs preferentially around the edge of a marginal sea, so that it is the effective volume that is fed directly. As we have suggested, this process would tend to be buffered to a lesser extent.

5. Summary

Overflow of dense water from the Nordic Seas to the Atlantic Ocean is a main driver of the lower limb of the AMOC. There has been a great interest in the stability of the overflow and its impact on the AMOC (Dickson et al. 2008). The Nordic Seas as a large reservoir has been considered as a stabilizing factor for the overflow stability. In this study we use a numerical model and an analytical water-mass budget model to show that the reservoir has a much smaller effective capacity and its stabilizing effect may be considerably weaker than previously thought. In a bowl-shape idealized basin or in a realistic Nordic Seas, the overflow draws its transport in the upstream basin along the geostrophic contours. The vast majority of the dense water is stored in the deep basin and often inside closed geostrophic contours. External forcing or ageostrophic processes are needed to unlock the reservoir storage in those regions. The wind stress in the Nordic Seas has a positive curl. It forces the convergence of the dense water toward the basin's interior and is against the drainage of the dense water there. So the wind stress forcing actually reduces the effective capacity. Mass fluxes by eddies to the overflow-feeding boundary current are only effective initially. As the water mass is drawn, the boundary-to-interior tilt of the isopycnal flattens if there is no robust renewal of the dense water mass. The boundary current therefore becomes more stable as the shear weakens.

In this study we consider an extreme scenario when the formation of the dense water is shut down or substantially weakened. In the present state, however, the dense water is renewed continuously, such as in the Lofoten and Norwegian Basins (Isachsen et al. 2007). The geostrophic buffering is still effective for the dense water that is stored in the deep basins. But it can be overcome by eddies as shown by Spall (2010). The buffering, however, becomes ineffective when the deep convection occurs over shelf or continental slope.

In summary, the effective capacity of the Nordic Seas as a dense-water reservoir for overflow is much smaller than what was estimated previously. This implies that the overflow transport is more responsive to climate changes in the Nordic Seas.

REFERENCES

Borenäs, K. M., and P. A. Lundberg, 1986: Rotating hydraulics of flow in a parabolic channel. *J. Fluid Mech.,* **167,** 309–326.

——, and ——, 1988: On the deep-water flow through the Faroe Bank Channel. *J. Geophys. Res.,* **93** (C2), 1281–1292.

Dickson, R., J. Meincke, and P. Rhines, 2008: Arctic-Subarctic ocean fluxes: Defining the role of the Northern Seas in climate. *Arctic-Subarctic Ocean Flux,* R. R. Dickson, J. Meincke, and P. Rhines, Eds., Springer, 1–12.

Girton, J. B., L. Pratt, D. Sutherland, and J. F. Price, 2006: Is the Faroe Bank Channel overflow hydraulically controlled? *J. Phys. Oceanogr.,* **36,** 2340–2349.

Hansen, B., and S. Østerhus, 2000: North Atlantic-Nordic Seas exchanges. *Prog. Oceanogr.,* **45,** 109–208.

——, and ——, 2007: Faroe Bank Channel overflow 1995-2005. *Prog. Oceanogr.,* **75,** 817–856.

——, ——, W. R. Turrell, S. Jonsson, H. Valdimarsson, H. Hatun, and S. M. Olsen, 2008: The inflow of Atlantic water, heat and salt to the Nordic Seas across the Greenland-Scotland Ridge. *Arctic-Subarctic Ocean Flux,* R. R. Dickson, J. Meincke, and P. Rhines, Eds., Springer, 15–43.

Isachsen, P. E., C. Mauritzen, and H. Svendsen, 2007: Dense water formation in the Nordic Seas diagnosed from sea surface buoyancy fluxes. *Deep-Sea Res. I,* **54,** 22–41.

Jonsson, S., 1991: Seasonal and interannual variability of wind stress curl over the Nordic Seas. *J. Geophys. Res.,* **96,** 2649–2659.

Käse, R. H., 2006: A Riccati model for Denmark Strait overflow variability. *Geophys. Res. Lett.,* **33,** L21S09, doi:10.1029/2006GL026915.

——, N. Serra, A. Köhl, and D. Stammer, 2009: Mechanisms for the variability of dense water pathways in the Nordic Seas. *J. Geophys. Res.,* **114,** C01012, doi:10.1029/2008JC004916.

Killworth, P. D., 1992: Flow properties in rotating, stratified hydraulics. *J. Phys. Oceanogr.,* **22,** 997–1017.

Nikolopoulos, A., K. Borenas, R. Hietala, and R. Lundberg, 2003: Hydraulic estimates of the Denmark Strait overflow. *J. Geophys. Res.,* **108,** 3095, doi:10.1029/2001JC001283.

Nøst, O. A., and P. E. Isachsen, 2003: The large-scale time-mean ocean circulation in the Nordic Seas and Arctic Ocean estimated from simple dynamics. *J. Mar. Res.,* **61,** 175–210.

Olsen, S. M., B. Hansen, D. Quadfasel, and S. Østerhus, 2008: Observed and modeled stability of overflow across the Greenland-Scotland ridge. *Nature,* **455,** 519–522, doi:10.1038/nature07302.

Pratt, L. J., and J. Whitehead, 2008: *Rotating Hydraulics*. Springer, 582 pp.

Price, J. F., and M. O. Baringer, 1994: Outflows and deep water production by marginal seas. *Prog. Oceanogr.,* **33,** 161–200.

Serra, N., R. H. Kase, A. Kohl, D. Stammer, and D. Quadfadsel, 2010: On the low-frequency phase relation between the Denmark Strait and the Faroe-Bank Channel overflows. *Tellus,* **62A,** 530–550.

Spall, M., 2004: Boundary currents and water mass transformation in marginal seas. *J. Phys. Oceanogr.,* **34,** 1197–1213.

——, 2010: Non-local topographic influences on deep convection: An idealized model for the Nordic Seas. *Ocean Modell.,* **32,** 72–85.

Whitehead, J. A., A. Leetma, and R. A. Knox, 1974: Rotating hydraulics of strait and sill flows. *Geophys. Fluid Dyn.,* **6,** 101–125.

Yang, J., and J. F. Price, 2000: Water mass formation and potential vorticity balance in an abyssal ocean circulation model. *J. Mar. Res.,* **58,** 789–808.

——, and ——, 2007: Potential vorticity constraint on the flow between two basins. *J. Phys. Oceanogr.,* **37,** 2251–2266.

Yu, L., X. Jin, and R. A. Weller, 2008. Multidecade global flux datasets from the Objectively Analyzed Air-Sea Fluxes (OAFlux) project: Latent and sensible heat fluxes, ocean evaporation, and related surface meteorological variables. Woods Hole Oceanographic Institution OAFlux Project Tech. Rep. OA-2008-01, 64 pp.